Biochemical and Biophysical Research Communications 484 (2017) 390–395

Contents lists available at ScienceDirect

Biochemical and Biophysical Research Communications

journal homepage: www.elsevier.com/locate/ybbrc

AvrXa27 binding influences unwinding of the double-stranded DNA in the *UPT* box

Jing Zhao [b, 1], Bo Zhang [a, 1], Junpeng Jiang [a], Nanv Liu [a], Qi Wei [a], Xuguang Xi [a], Jing Fu [a, *]

[a] State Key Laboratory of Crop Stress Biology for Arid Areas and College of Life Sciences, Northwest A&F University, Yangling, Shaanxi, People's Republic of China

[b] State Key Laboratory of Crop Stress Biology for Arid Areas and College of Plant Protection, Northwest A&F University, Yangling, Shaanxi, People's Republic of China

ARTICLE INFO

Article history:
Received 20 December 2016
Accepted 23 January 2017
Available online 26 January 2017

Keywords:
TAL
Binding affinity
Helicase
Transcriptional activation

ABSTRACT

Transcription-Activator Like (TAL) effectors, delivered by *Xanthomonas* pathogens bind specifically to *UP*-regulated by TAL effectors (*UPT*) box of the host gene promoter to arouse disease or trigger defense response. This type of protein-DNA interaction model has been applied in site-directed genome editing. However, the off-target effects of TAL have severely hindered the development of this promising technology. To better exploit the specific interaction and to deeper understand the TAL-induced host transcription rewiring, the binding between the central repeat region (CRR) of the TAL effector AvrXa27 and its *UPT* box variants was studied by kinetics analysis and TAL-blocked helicase unwinding assay. The results revealed that while AvrXa27 exhibited the highest affinity to the wild type *UPT* box, it could also bind to mutated *UPT* box variants, implying the possibility of non-specific interactions. Furthermore, some of these non-specific combinations restricted the helicase-elicited double-stranded DNA (dsDNA) separation to a greater extent. Our findings provide insight into the mechanism of TAL transcriptional activation and are beneficial to TAL-mediated genome modification.

1. Introduction

Pathogen derived Transcription-Activator Like (TAL) effectors alter host plant target gene expression by imitating eukaryotic transcription factors [1–5]. TAL effectors share a highly conserved structure, containing an N-terminal Type III secretion signal, a central repeat region (CRR), C-terminal nuclear localization signals, and a transcriptional activation domain [6]. CRR consists of repeats with similar amino acid sequences. Crystal structure studies show that each repeat forms a helix-loop-helix motif, and several repeats fold into a right-handed superhelix wrapping around the target promoter element. The repeat-variable diresidue (RVD) in the loop specifies the nucleotides-amino acid contact [7,8]. A series of results from GUS reporter gene assays and electrophoretic mobility shift assays have been statistically analyzed to decipher the code for recognition between the RVDs and their target DNA nucleotides. Some RVDs are found to interact preferably with a particular nucleotide, while others can bind to multiple nucleotides but with different frequencies [9–14].

The unique nucleotide binding property of TAL effectors has been widely used in customizing proteins for DNA editing (including cleavage, modification and mutation of target gene), manipulation of gene transcription, and creation of broad-spectrum disease resistance crops [4,15–19]. However, some off-target issues have been reported when using this TAL-DNA binding model [20–24], which severely hinders the application of this promising technology.

Recent studies resorted to detecting the specificity of the TAL and *UPT* box interaction by measuring binding affinity. Meckleret al. [25] revealed that different RVDs contributed to TAL-DNA binding affinities in various orders. In another case, excessive DNA binding affinity was found to cause reduced TALEN specificity [26]. Moreover, a study concerning a Zinc-finger protein demonstrated that for a particular DNA site, the protein with the highest affinity did not show the highest specificity [27]. Therefore, details regarding the activation of host gene transcription by TAL effectors remain largely unknown, and more work should be conducted to elucidate

Abbreviations: TAL, Transcription-Activator Like; *UPT*, *UP*-regulated by TAL effectors; CRR, central repeat region; dsDNA, double-stranded DNA; RVD, repeat-variable diresidue; TALEN, TAL Effector Nuclease.

* Corresponding author.
E-mail address: jingfu@nwsuaf.edu.cn (J. Fu).

[1] Jing Zhao and Bo Zhang contributed equally to this work.

http://dx.doi.org/10.1016/j.bbrc.2017.01.130
0006-291X/

the kinetic mechanisms of the interaction between TAL effectors and *UPT* boxes.

Here, we performed a traditional DNA-binding reaction and a newly developed TAL-blocked BsPif1 unwinding assay to explore the interaction between the CRR of AvrXa27 (AvrXa27CRR) and its corresponding *UPT* boxes. We discovered unusual combination features, which allowed us to deduce a model of TAL-regulated gene expression.

2. Materials and methods

2.1. Construction of the plasmid encoding AvrXa27CRR protein

A 2.2-kb fragment was PCR amplified from a vector carrying full-length AvrXa27 cDNA sequence using PrimerSTAR (TaKaRa) and primers 5′-GGAATTCCATATGGCCGCGCAGGTGGATCTA (*Nde*I site underlined), and 5′-GCCCTCGAGTTAGTCGACAACGCGATGGGA CGTGCGTT (*Xho*I site underlined). The product was digested with *Nde*I and *Xho*I and inserted into protein expression vector pET15b (Novagen) to create pET15b-AvrXa27CRR, which encoded an N-terminal 6X-His affinity tag and the CRR of AvrXa27.

2.2. Protein expression and purification

The pET15b-AvrXa27CRR plasmid was transformed into *E. coli* strain BL21 (DE3) (Novagen). The overexpression of AvrXa27CRR was induced during the log phase (OD_{600} = 0.5) by 0.4 mM isopropyl-1-thio-β-D-galactopyranoside for 14 h at 18 °C. Cells cultures were collected by centrifugation. The pellets were resuspended in lysis buffer (20 mM Tris-HCl pH7.6, 300 mM NaCl, 5 mM Imidazole) and lysed via sonication. After centrifugation, the supernatant containing AvrXa27CRR was first purified by Ni^{2+}-affinity chromatography (QIAGEN), then loaded on a SP column (GE Healthcare) and eluted by a NaCl gradient (100–1000 mM). The target protein-containing fractions were concentrated and dialyzed against the storage buffer (20 mM Tris-HCl pH7.5, 400 mM NaCl, 10% Glycerol and 1 mM DTT). The final AvrXa27CRR had the purity of >90% (Fig. 1A) and was stored at −80 °C.

2.3. DNA substrates and DNA labeling

All oligonucleotides were purchased from Shanghai Sangon Biotech (Shanghai, China). The sequences and fluorescent labels of the oligonucleotides were listed in Supplementary Table 1. All the oligonucleotides were purified by high performance liquid chromatography. Each duplex DNA substrate with a 5′-end 15-nt poly (dT) single-strand tail was formed by annealing a 3′-end fluorescein labeled oligonucleotide and its partially complementary 5′-end hexachlorofluorescein labeled or unlabeled oligonucleotide. The complementary dsDNA region corresponded to the *UPT* box. The resulting 2 μM duplex was kept in a buffer containing 10 mM Tris-HCl pH8.0 and 50 mM NaCl, and stored at −20 °C.

2.4. DNA-binding reactions

The binding reactions between AvrXa27CRR and *UPT* box were performed in a 150 μl buffer containing 20 mM Tris-HCl pH8.0, 50 mM KCl, 2 mM $MgCl_2$, 1 mM DTT. The concentration of fluorescently labeled DNA substrates was 5 nM, while the AvrXa27CRR concentration ranged from 0 to 100 nM. The reactions were incubated at 25 °C for 5 min, after which the steady-state fluorescence polarization was recorded by Infinite F200 (TECAN). The binding dissociation constant (K_d) of the protein-DNA complex was calculated according to previously published method [28].

2.5. TAL-blocked BsPif1 unwinding assay

The TAL-blocked BsPif1 unwinding assay was implemented by the stopped-flow fluorescence measurements. Each DNA substrate in this assay contained a 5′-end poly (dT) single-strand tail, a central double-stranded *UPT* box and a 3′-end quenched fluorescence signal. 100 nM AvrXa27CRR and 4 nM duplex DNA substrates were pre-incubated at 25 °C for 5 min. 100 nM BsPif1 helicase was added to incubate for another 5 min. The mixture was drawn into syringe one. A second syringe was filled with the same reaction buffer (25 mM Tris-HCl pH7.5, 50 mM NaCl, 2 mM $MgCl_2$, 2 mM DTT) as syringe one and 1 mM ATP. After incubation, the liquids in two syringes were rapidly mixed to initiate the unwinding reaction. The fluorescence enhancement of fluorophore due to the BsPif1-catalyzed strand separation was continuously monitored by a Bio-Logic MOS-450/AF-CD spectrometer (Bio-Logic, France). Control experiments were performed under the same conditions in the absence of AvrXa27CRR. All the stopped-flow kinetic traces derived from an average of 8 individual traces. The kinetic traces were analyzed as described previously [29,30].

3. Results

3.1. Design of Xa27 UPT box variants

The RVDs in the TAL central repeats preferentially recognize one of the four bases [12,13]. The TAL-mediated genome targeting relies on this 'one RVD to one base' code. Four RVDs have been extensively used in base recognition: NI for adenine (A), NG for thymine (T), HD for cytosine (C) and NN for guanine (G) [15–18,20–24]. In AvrXa27CRR, there are four NIs (all for A), three NGs (one for T, two for A), two HDs (both for C), five NNs (three for G, two for A), two N*s (one for A, one for C), and one NS (for G) (Fig. 1B). *Xa27 UPT* box variants were obtained by mutating some of the bases to the less frequently recognized bases (NI A→C, NG T→A, HD C→A, HD

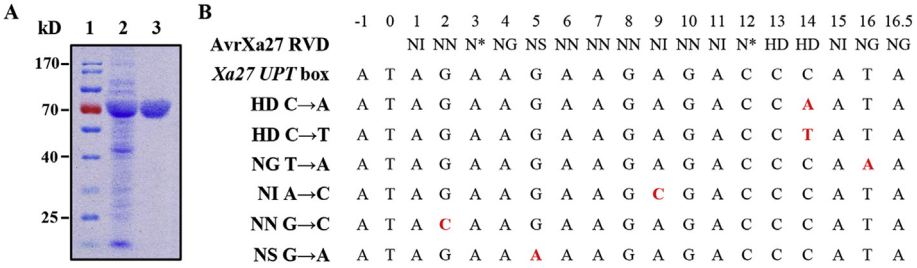

Fig. 1. AvrXa27CRR purification and design of *Xa27 UPT* box mutations. (A) SDS-PAGE analysis of the purified AvrXa27CRR. Lane 1, Molecular mass marker (kD); lane 2, supernatant of the cell extract; lane 3, purified AvrXa27CRR (3 μg). (B) Alignment of the *Xa27 UPT* box and variants. The mutated bases were presented in red and bold font. (For interpretation of the references to colour in this figure legend, the reader is referred to the web version of this article.)

Table 1
Binding constants of AvrXa27CRR for different DNA substrates.

DNA name	K_d (nM)	K_d Ratio (Mutant/WT)
Xa27 UPT box	0.36 ± 0.04	1.0
HD C→A	1.52 ± 0.36	4.2
HD C→T	1.14 ± 0.18	3.1
NG T→A	0.73 ± 0.08	2.0
NI A→C	1.46 ± 0.50	4.0
NN G→C	2.01 ± 0.63	5.5
NS G→A	1.48 ± 0.42	4.1

C→T, NN G→C, N* C→T), and one base to the more frequently recognized base (NS G→A) in light of the cipher deduced previously [12,13] (Fig. 1B). Original bases A in RVD position −1 and T in RVD position 0 preceding *Xa27 UPT* box were retained in all the tested sequences (Fig. 1B). All the oligonucleotide pairs formed stable duplex DNA substrates except the N* C→T pair, and N* was not a commonly used RVD for targeting, so the N* C→T variant was not studied in the following assays.

3.2. AvrXa27CRR binds to all the tested DNA substrates

AvrXa27CRR protein was expressed and purified to achieve the final purity above 90% (Fig. 1A). The ability of AvrXa27CRR binding to the *UPT* box DNA substrates was probed by the steady-state fluorescence anisotropy assay. The K_d value for each DNA substrate was determined based on fitting the data to the Michaelis-Menten equation, and could be used as an evaluation of the binding affinity between molecules. Generally, the K_d values of most sequence-specific DNA-binding proteins are in the nanomolar level or lower [31]. In contrast, proteins bind to non-specific DNA sequences with much higher K_d values [32]. Our results suggested that AvrXa27CRR bound to all the tested DNA substrates with K_d values varying from 0.36 ± 0.04 nM to 2.01 ± 0.63 nM (Table 1). Apparently, AvrXa27CRR displayed preference for the wild type *Xa27 UPT* box with the highest binding affinity (K_d value 0.36 ± 0.04 nM). The *Xa27 UPT* box variants exhibited an overall 2.0- to 5.5-fold reduction in AvrXa27CRR binding affinity. Among them, the variants NI A→C, NS G→A, HD C→A and NN G→C led to substantial reductions with relatively high K_d values (1.46 ± 0.50 nM to 2.01 ± 0.63 nM), whereas the variants NG T→A and HD C→T presented moderate reductions with intermediate K_d values (0.73 ± 0.08 nM and 1.14 ± 0.18 nM) (Fig. 2, Table 1).

3.3. AvrXa27CRR blocks the unwinding of Xa27 UPT box and variants

Transcription initiation begins with the binding of RNA polymerase and transcription factors to the promoter, followed by unwinding several base pairs of bound DNA region to form an open complex [33]. In order to investigate the effect of AvrXa27CRR on the unwinding of *UTP* boxes during the TAL-mediated transcriptional activation, a TAL-blocked helicase unwinding assay was introduced. BsPif1 DNA helicase, which unwound partial duplex DNA substrates with a 5′-overhang along the 5′-to-3′ direction, was used to conduct the unwinding assay [34]. In our experiment, each DNA substrate contained a 5′-end poly (dT) tail, a 19-bp *UPT* box double-stranded region and a 3′-end quenched fluorescence signal. Once the 3′-end quenched fluorophores were uncoupled from each other as a result of BsPif1 catalyzed unwinding, FRET signal could be detected. In the absence of AvrXa27CRR, the characteristic BsPif1 unwinding curves for all the DNA substrates were successfully obtained (Fig. 3). In the presence of AvrXa27CRR, reaction progress curves showed that the binding of AvrXa27CRR to all the tested

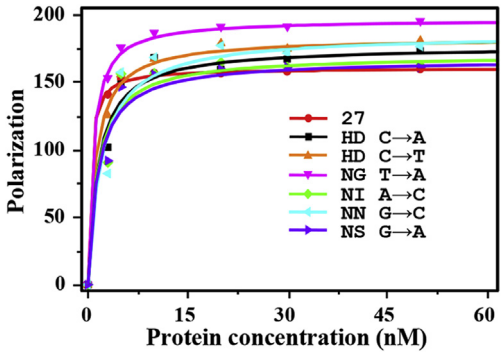

Fig. 2. The binding curves of AvrXa27CRR to all the tested DNA substrates. Fluorescence polarization as a function of AvrXa27CRR concentration for different DNA substrates.

DNA substrates effectively slowed down the overall unwinding progress (Fig. 3). The blocking effects fell into three categories (Table 2): (a) The binding of AvrXa27CRR to the variants NG T→A and NS G→A as well as the wild type *Xa27 UPT* box blocked the unwinding to a slight extent (1.5- to 2.8-fold reduction in the reaction rate); (b) The binding to the variant HD C→T caused a little higher blocking response (4.2-fold reduction in the reaction rate); (c) The binding to the variants NI A→C, NN G→C and HD C→A provoked extremely strong blocking effect (5.9- to 12.8-fold reduction in the reaction rate). In a word, once the recognized bases of three (NI, NN and HD) out of the four most regular RVDs for targeting were mutated, AvrXa27CRR would become more difficult to separate from the *UPT* boxes during the dsDNA unwinding.

4. Discussion

TAL effectors are shrewd tools for pathogens to remodel host plants for their own benefits of infection and propagation [35,36]. The excellent binding specificity of TAL effectors to the *UPT* box DNA brings hope and inspiration for genome engineering. However, an increasing number of reported off-target occurrences in TALEN-mediated gene editing urge scientists to find out more direct quantitative evaluations of TAL and target DNA interaction.

In this study, the affinity of AvrXa27CRR and different *UPT* boxes was tested by a traditional kinetic analysis. The wild type *Xa27 UPT* box was the most optimal substrate for AvrXa27CRR, as all variants showed declined binding affinities (Fig. 2, Table 1), which conformed to the one-to-one correspondence rule for RVDs and target nucleotides [12,13]. However, the K_d values for the interactions between AvrXa27CRR and *UPT* variants in our study were still at a relatively low level compared with those in other related studies (Fig. 2, Table 1) [25,31,32]. These results suggested that besides its favorite DNA sequence, AvrXa27CRR could also bind other dsDNA with similar sequence.

A previously well-studied bacteriophage T4 Dda helicase could displace the *E. coli trp* repressor from the *trpEDCBA* operator and unwind the duplex DNA substrate. The binding of *trp* repressor to the operator decreased the unwinding rate of Dda helicase [37]. Similarly, our results suggested that the binding of AvrXa27CRR to the wild type *Xa27 UPT* box and variants could postpone the BsPif1 unwinding reaction (Fig. 3, Table 2). Surprisingly, binding of AvrXa27CRR to the wild type *Xa27 UPT* box was not the strongest obstacle to impede BsPif1 unwinding. On the contrary, binding to some variants (NI A→C, NN G→C, HD C→A and HD C→T) caused more potent constraint on dsDNA separation (Fig. 3, Table 2). We postulated that the interaction between TAL effectors and mutated *UPT* sequences may significantly inhibit the dsDNA unwinding

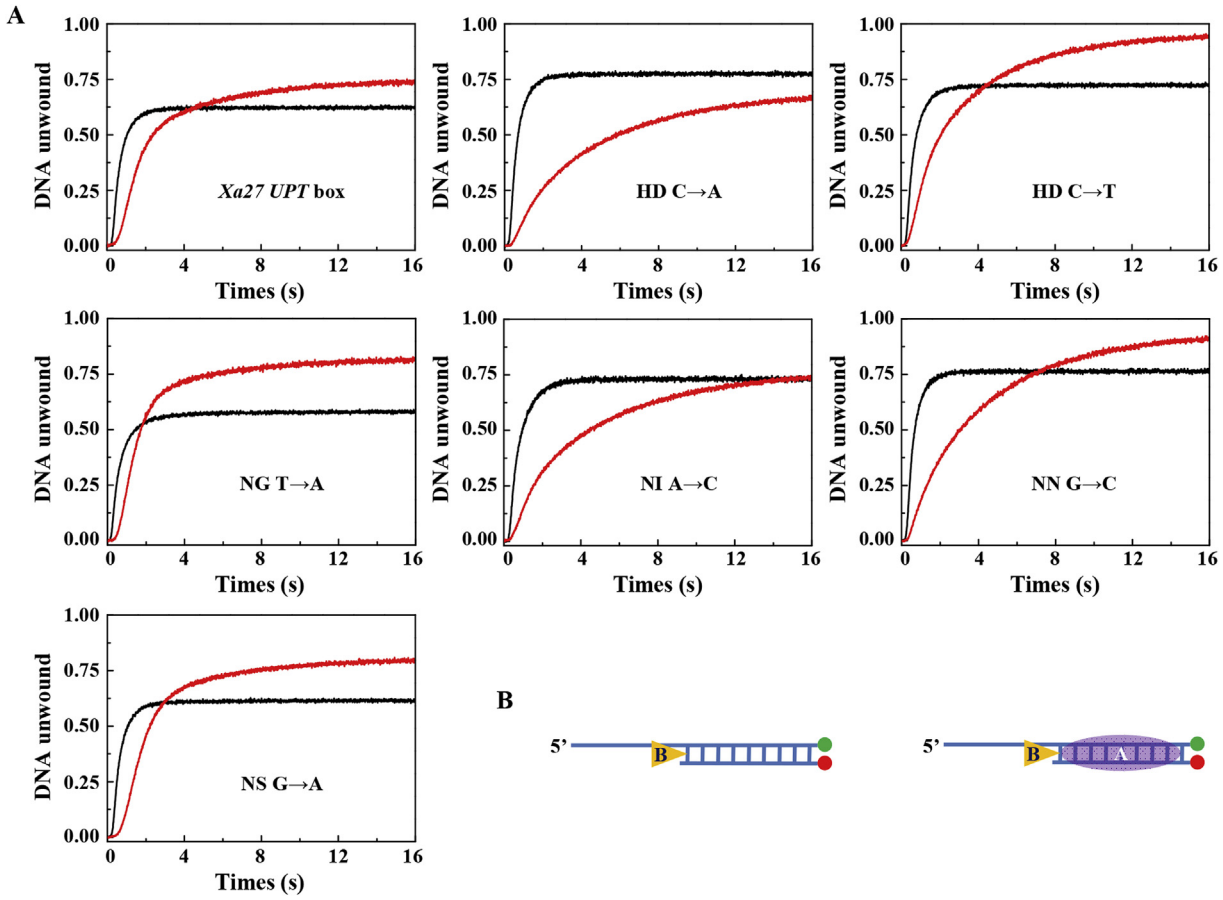

Fig. 3. The blocking effect of AvrXa27CRR on the BsPif1-mediated DNA unwinding. (A) Time courses of BsPif1 unwinding in the presence and absence of AvrXa27CRR. Curves in black represented BsPif1 alone unwinding reaction progresses, and curves in red represented BsPif1 unwinding reaction progresses in the presence of AvrXa27CRR. (B) A schematic diagram of AvrXa27CRR blocked BsPif1 unwinding. The duplex DNA substrate (blue) was labeled with fluorescent donor fluorescein (green circle) and acceptor hexachlorofluorescein (red circle) at the 3′-end. The 5′-overhang was composed of a 15-nt poly (dT), and a double-strands region denoted the 19-bp *Xa27 UPT* box or its variants. The yellow triangle and purple oval typified BsPif1 and AvrXa27CRR, respectively. (For interpretation of the references to colour in this figure legend, the reader is referred to the web version of this article.)

during transcription initiation, leading to transcriptional repression of downstream genes. This could be supported by transient promoter GUS assays in *Nicotiana benthamiana*, which demonstrated that the GUS reporter would be inactivated once the most favorite bases of RVDs HD (C), NI (A), and NN (G and A) were mutated to other bases [13]. In addition, our result suggested that the effect of AvrXa27CRR on the separation of variant NS G→A and the wild type Xa27 *UPT* box was similar (Fig. 3, Table 2), which was also consistent with the observation that mutations of RVD NS's favorite base did not change the GUS activity [13].

Based on all these results, we propose a TAL-mediated transcriptional activation model, as stated below. TAL effectors

Table 2
Unwinding parameters for different DNA substrates in the presence and absence of AvrXa27CRR.

	AvrXa27	A_1[a]	$k_{obs,1}$[b] (s^{-1})	Rate (s^{-1}) ($A_1 \times k_{obs,1}$)	Blocking Fold [Rate (−)/Rate (+)]
Xa27 UPT box	-	0.69 ± 0.03	2.03 ± 0.06	1.40 ± 0.04	2.8
	+	0.68 ± 0.02	0.73 ± 0.02	0.50 ± 0.01	
HD C→A	-	0.83 ± 0.03	2.16 ± 0.07	1.79 ± 0.01	12.8
	+	0.18 ± 0.01	0.76 ± 0.07	0.14 ± 0.01	
HD C→T	-	0.76 ± 0.03	2.09 ± 0.09	1.58 ± 0.00	4.2
	+	0.44 ± 0.02	0.88 ± 0.05	0.38 ± 0.00	
NG T→A	-	0.47 ± 0.03	2.35 ± 0.11	1.09 ± 0.02	1.5
	+	0.79 ± 0.02	0.91 ± 0.02	0.72 ± 0.00	
NI A→C	-	0.65 ± 0.09	1.82 ± 0.17	1.17 ± 0.06	5.9
	+	0.25 ± 0.01	0.83 ± 0.03	0.20 ± 0.00	
NN G→C	-	0.80 ± 0.03	2.34 ± 0.06	1.87 ± 0.02	11.7
	+	0.19 ± 0.02	0.85 ± 0.04	0.16 ± 0.01	
NS G→A	-	0.67 ± 0.04	2.09 ± 0.12	1.39 ± 0.04	2.5
	+	0.80 ± 0.01	0.70 ± 0.00	0.56 ± 0.00	

[a] A_1 indicated the unwinding amplitude of the fast phase.
[b] $k_{obs,1}$ indicated the observed kinetic rate of the fast phase.

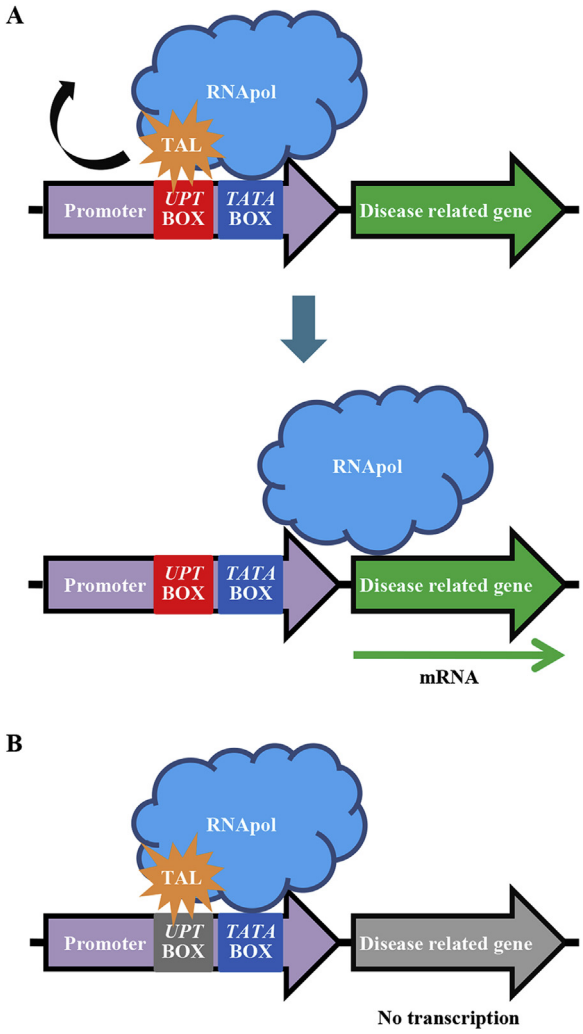

Fig. 4. Model depicting TAL-mediated transcriptional activation. (A) The binding of TAL to the wild type *UPT* box activates transcription. (B) The binding of TAL to the non-specific *UPT* box represses transcription. The red *UPT* box and grey *UPT* box symbolize the wild type *UPT* box and mutated *UPT* box, respectively. (For interpretation of the references to colour in this figure legend, the reader is referred to the web version of this article.)

preferentially bind to the wild type *UPT* box with less constraint on the unwinding of dsDNA, thus allowing for the recruitment of RNA polymerase and transcription activation of downstream genes (Fig. 4A). TAL effectors can also bind to non-specific *UPT* boxes (Fig. 2, Table 1), but in this case dsDNA unwinding will be significantly reduced, consequently resulting in shutdown of downstream genes (Fig. 4B).

The off-target problems of TALENs can be partly illustrated by our model. TALENs can bind to homologous off-target sites, leading to non-specific cleavage, especially when expressed at a high concentration. Besides the one-to-one cipher, therefore, homologous sites should be avoided as much as possible in TALENs design.

In conclusion, our results suggest that most atypical mutations in the *Xa27 UPT* box decrease the affinity of binding by AvrXa27CRR. However, once AvrXa27CRR binds to mutated *Xa27UPT* box, their interaction will interfere with dsDNA separation, which is a critical step in transcription initiation, particularly for open complex formation. Our findings thus advance the understanding of the mechanisms underlying TAL-mediated transcriptional activation and the occurrence of TALEN-induced off-target events.

Acknowledgements

This work was supported by the National Natural Science Foundation of China (31301632), the Fundamental Research Funds for the Central Universities (2452015075, 2452015418), and the Doctoral Starting up Foundation of Shaanxi province, China (Z109021115). We thank Professor Yin Zhongchao (Temasek Life Sciences Laboratory, Singapore) for providing the vector carrying full-length AvrXa27 cDNA sequence and Dr. Cui Hongchang (Department of Biological Science, Florida State University, USA) for reviewing the manuscript.

Appendix A. Supplementary data

Supplementary data related to this article can be found at http://dx.doi.org/10.1016/j.bbrc.2017.01.130.

Transparency document

Transparency document related to this article can be found online at http://dx.doi.org/10.1016/j.bbrc.2017.01.130.

References

[1] K.Y. Gu, B. Yang, D.S. Tian, et al., R gene expression induced by a type-III effector triggers disease resistance in rice, Nature 435 (2005) 1122–1125.
[2] Z.H. Chu, M. Yuan, L.L. Yao, et al., Promoter mutations of an essential gene for pollen development result in disease resistance in rice, Gene Dev. 20 (2006) 1250–1255.
[3] B. Yang, A. Sugio, F.F. White, Os8N3 is a host disease-susceptibility gene for bacterial blight of rice, Proc. Natl. Acad. Sci. U. S. A. 103 (2006) 10503–10508.
[4] P. Romer, S. Recht, T. Lahaye, A single plant resistance gene promoter engineered to recognize multiple TAL effectors from disparate pathogens, Proc. Natl. Acad. Sci. U. S. A. 106 (2009) 20526–20531.
[5] P. Romer, T. Strauss, S. Hahn, et al., Recognition of AvrBs3-like proteins is mediated by specific binding to promoters of matching pepper Bs3 alleles, Plant Physiol. 150 (2009) 1697–1712.
[6] S. Schornack, A. Meyer, P. Romer, et al., Gene-for-gene-mediated recognition of nuclear-targeted AvrBs3-like bacterial effector proteins, J. Plant Physiol. 163 (2006) 256–272.
[7] D. Deng, C.Y. Yan, X.J. Pan, et al., Structural basis for sequence-specific recognition of DNA by TAL effectors, Science 335 (2012) 720–723.
[8] A.N.S. Mak, P. Bradley, R.A. Cernadas, et al., The crystal structure of TAL effector PthXo1 bound to its DNA target, Science 335 (2012) 716–719.
[9] S. Kay, S. Hahn, E. Marois, et al., A bacterial effector acts as a plant transcription factor and induces a cell size regulator, Science 318 (2007) 648–651.
[10] P. Romer, S. Hahn, T. Jordan, et al., Plant pathogen recognition mediated by promoter activation of the pepper Bs3 resistance gene, Science 318 (2007) 645–648.
[11] S. Kay, S. Hahn, E. Marois, et al., Detailed analysis of the DNA recognition motifs of the Xanthomonas type III effectors AvrBs3 and AvrBs3 Delta rep16, Plant J. 59 (2009) 859–871.
[12] M.J. Moscou, A.J. Bogdanove, A simple cipher governs DNA recognition by TAL effectors, Science 326 (2009), 1501–1501.
[13] J. Boch, H. Scholze, S. Schornack, et al., Breaking the code of DNA binding specificity of TAL-type III effectors, Science 326 (2009) 1509–1512.
[14] T. Yuan, X.H. Li, J.H. Xiao, et al., Characterization of Xanthomonas oryzae-responsive cis-acting element in the promoter of rice race-specific susceptibility gene Xa13, Mol. Plant 4 (2011) 300–309.
[15] J.C. Miller, S.Y. Tan, G.J. Qiao, et al., A TALE nuclease architecture for efficient genome editing, Nat. Biotechnol 29 (2011) 143–149.
[16] M.M. Mahfouz, L.X. Li, M. Shamimuzzaman, et al., De novo-engineered transcription activator-like effector (TALE) hybrid nuclease with novel DNA binding specificity creates double-strand breaks, Proc. Natl. Acad. Sci. U. S. A. 108 (2011) 2623–2628.
[17] T. Li, S. Huang, W.Z. Jiang, et al., TAL nucleases (TALNs): hybrid proteins composed of TAL effectors and FokI DNA-cleavage domain, Nucleic Acids Res. 39 (2011) 359–372.
[18] A.J. Bogdanove, D.F. Voytas, TAL effectors: customizable proteins for DNA targeting, Science 333 (2011) 1843–1846.
[19] A.W. Hummel, E.L. Doyle, A.J. Bogdanove, Addition of transcription activator-like effector binding sites to a pathogen strain-specific rice bacterial blight resistance gene makes it effective against additional strains and against bacterial leaf streak, New Phytol. 195 (2012) 883–893.
[20] C. Mussolino, R. Morbitzer, F. Lutge, et al., A novel TALE nuclease scaffold enables high genome editing activity in combination with low toxicity, Nucleic Acids Res. 39 (2011) 9283–9293.

[21] T.J. Dahlem, K. Hoshijima, M.J. Jurynec, et al., Simple methods for henerating and fetecting locus-dpecific mutations induced with TALENs in the zebrafish genome, PLoS Genet. 8 (2012).
[22] L. Tesson, C. Usal, S. Menoret, et al., Knockout rats generated by embryo microinjection of TALENs, Nat. Biotechnol. 29 (2011) 695–696.
[23] D. Hockemeyer, H.Y. Wang, S. Kiani, et al., Genetic engineering of human pluripotent cells using TALE nucleases, Nat. Biotechnol. 29 (2011) 731–734.
[24] M.J. Osborn, C.G. Starker, A.N. McElroy, et al., TALEN-based gene correction for Epidermolysis bullosa, Mol. Ther. 21 (2013) 1151–1159.
[25] J.F. Meckler, M.S. Bhakta, M.S. Kim, et al., Quantitative analysis of TALE-DNA interactions suggests polarity effects, Nucleic Acids Res. 41 (2013) 4118–4128.
[26] J.P. Guilinger, V. Pattanayak, D. Reyon, et al., Broad specificity profiling of TALENs results in engineered nucleases with improved DNA-cleavage specificity, Nat. Methods 11 (2014) 429–435.
[27] D. Jantz, J.M. Berg, Probing the DNA-binding affinity and specificity of designed zinc finger proteins, Biophys. J. 98 (2010) 852–860.
[28] W. Qin, N.N. Liu, L.J. Wang, et al., Characterization of biochemical properties of Bacillus subtilis RecQ Helicase, J. Bacteriol. 196 (2014) 4216–4228.
[29] N.N. Liu, X.L. Duan, X. Ai, et al., The Bacteroides sp. 3_1_23 Pif1 protein is a multifunctional helicase, Nucleic Acids Res. 43 (2015) 8942–8954.
[30] X.D. Zhang, S.X. Dou, P. Xie, et al., Escherichia coli RecQ is a rapid, efficient, and monomeric helicase, J. Biol. Chem. 281 (2006) 12655–12663.
[31] N. Nunez, M.M.K. Clifton, A.P.W. Funnell, et al., The multi-zinc finger protein ZNF217 contacts DNA through a two-finger domain, J. Biol. Chem. 286 (2011) 38190–38201.
[32] J. Iwahara, M. Zweckstetter, G.M. Clore, NMR structural and kinetic characterization of a homeodomain diffusing and hopping on nonspecific DNA, P. Natl. Acad. Sci. U. S. A. 103 (2006) 15062–15067.
[33] C. Plaschka, M. Hantsche, C. Dienemann, et al., Transcription initiation complex structures elucidate DNA opening, Nature 533 (2016) 353–358.
[34] X.L. Duan, N.N. Liu, Y.T. Yang, et al., G-quadruplexes significantly stimulate Pif1 helicase-catalyzed duplex DNA unwinding, J. Biol. Chem. 290 (2015) 7722–7735.
[35] Y. Saijo, P. Schulze-Lefert, Manipulation of the eukaryotic transcriptional machinery by bacterial pathogens, Cell Host Microbe 4 (2008) 96–99.
[36] H. Scholze, J. Boch, TAL effectors are remote controls for gene activation, Curr. Opin. Microbiol. 14 (2011) 47–53.
[37] A.K. Byrd, K.D. Raney, Displacement of a DNA binding protein by Dda helicase, Nucleic Acids Res. 34 (2006) 3020–3029.